INSTITUTE OF PHYSICS PUBLISHING INVERSE PROBLEMS

Inverse Problems **22** (2006) 645–661 doi:10.1088/0266-5611/22/2/016

An inverse problem in nondestructive evaluation of spot-welds

Elisa Francini[1], **Thomas Höft**[2] **and Fadil Santosa**[2]

[1] Istituto per le Applicazione del Calcolo—Sezione di Firenze, Via Madonna del Piano, CNR Edificio F, 50019 Sesto Fiorentino, Italy
[2] School of Mathematics, University of Minnesota, 127 Vincent Hall, 206 Church St SE, Minneapolis, MN 55455, USA

Received 18 October 2005, in final form 1 March 2006
Published 27 March 2006
Online at stacks.iop.org/IP/22/645

Abstract
In this work, we investigate the problem of determining a heat source at the bottom of a plate from thermal measurements obtained at the top. This problem arises in a novel nondestructive evaluation technique for assessing the quality of a spot-weld. We devise a simple algorithm that takes thermal images and produces estimates of the heat source. The computational approach, which uses Tikhonov regularization, is shown to be convergent. Numerical examples illustrate the behaviour of the inversion algorithm.

1. Introduction

Spot-welds are commonly used in the automotive industry to join metal sheets. To create a spot-weld between two metal sheets, the sheets are first clamped together. A large amount of electrical current is allowed to pass at the location where the weld is desired. The current basically melts the metal, creating a weld nugget joining the two sheets. The quality of the weld, measured by its strength, is affected by the electrodes responsible for the currents. A nondestructive evaluation method for assessing the quality of a spot-weld is of great interest.

The technique described in this work was devised by Dr Cameron Dasch of General Motors Research. The method is similar to the crack imaging method developed by Favro *et al* [3, 4, 6]. The set-up is sketched in figure 1. An ultrasonic transducer is attached to the surface of one of the sheets. It generates vibrations in the sample which cause the two sheets to rub against each other. The friction forces, which generate heat between the two sheets, are expected to be strongest near the weld. Thus the area between the sheets surrounding the weld is a heat source, generating a temperature change. As the heat is conducted to the top surfaces of the two sheets, temperature changes are captured with an infrared camera. Because the areas surrounding a weld act like a heat source, the captured thermal image is expected to be brightest near the weld. It is from these thermal images that one would like to obtain an assessment of the weld quality.

 © 2006 IOP Publishing Ltd Printed in the UK

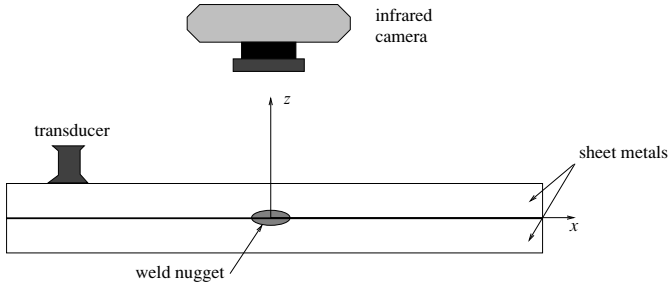

Figure 1. A schematic of the nondestructive evaluation technique. A piezoelectric transducer vibrates the sheets. Friction causes the plates to heat up, with most heat being generated near the weld. An infrared camera reads the temperature change on the surface. The temperature image provides an estimate of the properties of the weld.

The present paper provides a solution for the first part of this problem, that of determining the heat source between the two joined metal sheets. The source is a surface flux which depends on time. We do not address the important issue of correlating the heat source with weld quality. Such an effort will require modelling heat generation from friction.

Our approach to determining the heat source starts by modelling the heat conduction problem. The three-dimensional (3D) model is further simplified to a two-dimensional (2D) model by assuming that the metal sheets being welded are thin. For this problem, temperature data on the surface of the plate are measured at regular time intervals. The temperature on the surface consists of two parts: (i) conducted temperature, (ii) temperature change caused by the heat source. The contributions from each part can be represented by linear operators. The inverse problem amounts to finding the heat source responsible for the temperature change between the two times. This means that to solve it, one must invert a compact operator.

To further simplify our problem, we assume that the heat source is time independent between time samples. This, together with the Tikhonov regularization, allows us to reconstruct the heat source by solving a simple linear system. The errors in the reconstruction will consist of two parts. First, if there is noise in the data, the reconstruction will be affected by it. Second, we make an error in assuming that the source is time independent between time samples. To address the issue of reconstruction error, we devise error estimates, which can be interpreted to show that convergence is achieved, under suitable hypotheses, if the noise level and the time sample increment go to zero.

The paper is organized as follows. We provide a precise description of the problem in section 2. Reduction to a 2D problem by exploiting the fact that the plate is thin is given in section 3. In section 4 we recast the inverse problem as that of solving an integral equation of the first kind. We show how the solution of this equation can be approximated by using Tikhonov regularization, and describe a computational method for doing so. Estimates of the reconstruction error caused by data noise and further approximation are established in section 5. Numerical examples are given in section 6 to illustrate the behaviour of the computational approach. The paper ends with a short discussion.

2. Problem formulation and modelling

We consider the simple case of two identical sheets that have been joined by welding. Symmetry allows us to consider just one sheet (see figure 2). The plate-like domain in

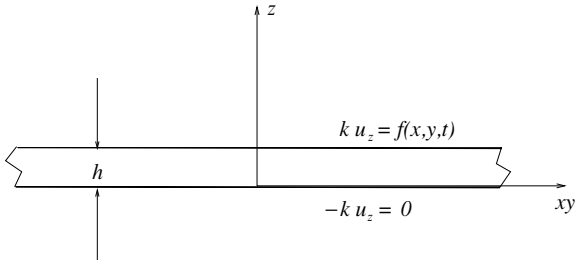

Figure 2. We consider only one of the two metal sheets. Friction causes heat to be generated near the weld. This is modelled by a flux boundary condition on the top side of the plate. The bottom of the plate is insulated. Temperature measurements are taken on the insulated side.

which heat conduction takes place is $\Omega = [0, h] \times \mathbb{R}^2$, where h is the plate thickness. Let $u(x, y, z, t)$ represent the difference between the temperature in the plate and the ambient air temperature. Then u satisfies

$$u_t = \kappa \Delta u, \qquad (x, y, z) \in \Omega, \quad t > 0, \tag{1}$$

where κ is the diffusivity. The initial temperature of the plate is assumed to be the same as that of the ambient air, therefore

$$u(x, y, z, 0) = 0.$$

When the transducer is turned on, vibrations are generated in the plates. Friction between the two plates causes heat to be generated near the weld. We model this as a heat flux on the top side of the plate under consideration,

$$ku_z(x, y, h, t) = f(x, y, t), \qquad (x, y) \in \mathbb{R}^2, \quad t > 0, \tag{2}$$

where k is the conductivity of the metal. It is assumed that $f(x, y, t \leqslant 0) = 0$. The bottom side of the plate is exposed to air. The temperature change caused by the heat source is assumed to be sufficiently small that the bottom boundary can be modelled as being insulated. Therefore we have

$$-ku_z(x, y, 0, t) = 0, \qquad (x, y) \in \mathbb{R}^2, \quad t > 0. \tag{3}$$

In the problem, the source $f(x, y, t)$ is unknown. On the other hand, we are given measurement of temperature on the bottom of the plate

$$u(x, y, 0, t) = g(x, y, t). \tag{4}$$

The inverse problem then is to determine $f(x, y, t)$ given that $u(x, y, 0, t) = g(x, y, t)$. We also have an additional piece of information about the source. The piezoelectric transducer is turned off after a short time, thus no heat is generated after it has been turned off. Therefore $f(x, y, t > t^*) = 0$ for some known t^*.

3. Thin plate approximation

Since the plate is very thin, in real terms and in relative terms (to be specified below), we want to exploit this fact to simplify the problem. We start by decomposing the temperature u into two parts so that we can consider a problem with homogeneous boundary conditions. Let $u = v + w$ where

$$w(x, y, z, t) = \frac{z^2}{2kh} f(x, y, t).$$

Substituting this expression for u in (1) we find that $v(x, y, z, t)$ satisfies an inhomogeneous heat equation

$$v_t = \kappa \Delta v + \left(\frac{z^2}{2kh} [-f_t + \kappa \Delta_{xy} f] + \frac{\kappa}{kh} f \right).$$

Since w satisfies the boundary conditions for u in (2)–(3), it is easy to see that v satisfies homogeneous Neumann boundary conditions

$$v_z(x, y, 0, t) = v_z(x, y, h, t) = 0.$$

We can now expand v in Fourier series

$$v(x, y, z, t) = \sum_{n=0}^{\infty} A_n(x, y, t) \cos \frac{n\pi z}{h}.$$

Substituting this expansion in the heat equation satisfied by v leads to

$$A_{n,t} = \kappa \Delta_{xy} A_n - \kappa \left(\frac{n\pi}{h} \right)^2 A_n + F_n(x, y, t). \tag{5}$$

The forcing terms are

$$F_n(x, y, t) = \begin{cases} \dfrac{h}{6k}(-f_t + \kappa \Delta_{xy} f) + \dfrac{\kappa}{kh} f, & n = 0, \\ \dfrac{2h}{n^2 \pi^2 k}(-f_t + \kappa \Delta_{xy} f) \cos n\pi, & n > 0. \end{cases}$$

We need to make (5) non-dimensional. To this end, let u_0 be a reference temperature, and ℓ_0 be a characteristic length. The characteristic length could be several multiples of the size of a typical spot-weld, which will make it much greater than the plate thickness. The non-dimensional distance is $x' = x/\ell_0$, non-dimensional time is $t' = t\kappa/\ell_0^2$, and the non-dimensional temperature is $A'_n = A_n/u_0$. After rescaling, (5) becomes

$$A'_{n,t'} = \Delta_{x'y'} A'_n - \left(\frac{\ell_0}{h} \right)^2 (n\pi)^2 A'_n + \frac{\ell_0^2}{\kappa u_0} F_n.$$

Of particular interest is the expression involving F_0. We obtain

$$\frac{\ell_0^2}{\kappa u_0} F_0 = \frac{h}{\ell_0} \frac{\ell_0}{6ku_0} [-f_{t'} + \Delta' f] + \frac{\ell_0}{h} \frac{\ell_0}{ku_0} f.$$

We assume that $\ell_0 \gg h$, and therefore, the first term on the right-hand side may be ignored. By the same token, the terms involving F_n for $n > 0$ are of the same size as the term just ignored, and shall be dropped. Indeed, one can see that A_n for $n > 0$ decays like $\exp(-(\ell_0/h)^2 (n\pi)^2 t')$ once $F_n(x, y, t)$ becomes zero.

Therefore, $A_0(x, y, t)$ is the leading term describing the behaviour of $v(x, y, z, t)$. The correction is of the order of h while $f(x, y, t) \neq 0$; exponentially small after $f(x, y, t)$ becomes zero. We only care about $u(x, y, 0, t)$, and

$$u(x, y, 0, t) = v(x, y, 0, t) \approx A_0(x, y, t).$$

With a little abuse of notation, we can now state our simplified inverse problem.

We have a two-dimensional temperature field $u(x, y, t)$ which satisfies the equation satisfied by A_0 (approximately),

$$u_t = \kappa \Delta_{xy} u + \frac{\kappa}{kh} f(x, y, t). \tag{6}$$

It is an approximation of the temperature of the three-dimensional field $u(x, y, z, t)$ satisfying (1) for $z = 0$. We are given data

$$u(x, y, t) = g(x, y, t). \tag{7}$$

The inverse problem is to determine $f(x, y, t)$ from (6)–(7). Thus, we have reduced the three-dimensional inverse problem described in the previous section to a two-dimensional one.

4. Inversion algorithm

In our problem, we assume that temperature readings are given at regular intervals of time. One way to look at the problem is to study what happens between a time interval and consider the relationship between the temperatures at the start and the end of the interval, and the heat source in that interval. This relationship is linear and can be easily expressed in terms of the heat kernel [7].

Let us assume that we work with times $t_0, t_1, \ldots, t_N$. Henceforth, we absorb the coefficients multiplying the unknown $f(x, y, t)$ in (6) into the unknown. Consider the initial value problem

$$u_t = \Delta_{xy} u + f(x, y, t), \quad t_k < t < t_{k+1}. \tag{8}$$

Note that we have also rescaled to remove κ from the equation. We study the mapping from $u(x, y, t_k)$ and $f(x, y, t)$ for $t_k \leqslant t < t_{k+1}$ to $u(x, y, t_{k+1})$. We can write the solution $u(x, y, t)$ of (8) using the heat kernel. In particular, we have

$$\begin{aligned} u(x, y, t_{k+1}) = &\int K(x - \xi, y - \eta, \Delta t) u(\xi, \eta, t_k)\, \mathrm{d}\xi\, \mathrm{d}\eta \\ &+ \int_0^{\Delta t} \int K(x - \xi, y - \eta, \Delta t - \tau) f(\xi, \eta, t_k + \tau)\, \mathrm{d}\xi\, \mathrm{d}\eta\, \mathrm{d}\tau, \end{aligned} \tag{9}$$

where $K(x, y, t)$ is the heat kernel, given by

$$K(x, y, t) = \frac{1}{4\pi t} \exp \frac{-(x^2 + y^2)}{4t}.$$

The equation relates the temperature at t_{k+1} to the temperature at t_k, and the heat source within the window $[t_k, t_{k+1})$. It states that the temperature at time t_{k+1} is related to the temperature at time t_k through the convolution with the heat kernel, and through Duhamel's principle with the source.

From this representation, we can see that our inverse problem amounts to estimating the heat source $f(x, y, t)$ in the interval $[t_k, t_{k+1})$ given the temperature readings at t_k and t_{k+1}. A quick parameter count convinces us that we cannot determine a function of three variables from two functions of two variables. However, we will assume that the sampling rate $\Delta t = (t_{k+1} - t_k)$ is small, which further justifies the approximation that $f(x, y, t)$ for $t \in [t_k, t_{k+1})$ is constant in t. Therefore, we write

$$f(x, y, t) = f_k(x, y), \qquad \text{for} \quad t_k \leqslant t < t_{k+1}.$$

We will later derive an error estimate for this approximation.

With this approximation, we can write (9) in shorthand notation as

$$u_{k+1} = K_0 u_k + K_1 f_k, \tag{10}$$

where $u_k(x, y) = u(x, y, t_k)$ and $u_{k+1} = u(x, y, t_{k+1})$. The operators K_0 and K_1 are convolutions with the heat kernel

$$k_0(x, y) = K(x, y, \Delta t),$$

and with

$$k_1(x, y) = \int_0^{\Delta t} K(x, y, \Delta t - \tau)\, \mathrm{d}\tau.$$

Given data (g_k, g_{k+1}) corresponding to temperatures at times t_k and t_{k+1}, we solve for f_k using Tikhonov regularization

$$f_k = \arg\min_{\phi} \|K_1\phi + K_0 g_k - g_{k+1}\|_2^2 + \alpha\|\phi\|_2^2. \tag{11}$$

Here α is the tuning parameter for the regularization.

The inversion algorithm we envision is sequential. We take data given at time t_0 and t_1, namely, g_0 and g_1 to find f_0. Then, g_1 and g_2 are used to find f_1, and so on. When we are finished, we have constructed a piecewise constant (in time) approximation of $f(x, y, t)$, given by $f_0, f_1, \ldots, f_{N-1}$. Solving (11) at each step requires solution of a potentially large linear system. We propose doing this by a conjugate gradient method.

5. Error estimates

We assume that we record the surface temperatures over the time horizon $[0, T]$, and $N + 1$ time samples of temperature are taken at regular intervals. In the inversion algorithm we proposed in the previous section, values of $f(x, y, t)$ for $t_k \leqslant t < t_{k+1}$ are estimated from the data at times t_k and t_{k+1}. We start by analysing this subproblem.

Let $f(x, y, t)$ be the actual source term in (8) in the time interval $[t_k, t_{k+1}]$, and let $g_k(x, y)$ and $g_{k+1}(x, y)$ be the measured values for the functions $u_k(x, y) = u(x, y, t_k)$ and $u_{k+1}(x, y) = u(x, y, t_{k+1})$. We assume that the error in the data is bounded by some known value δ, that is

$$\|u_k - g_k\|_2 \leqslant \delta \quad \text{and} \quad \|u_{k+1} - g_{k+1}\|_2 \leqslant \delta, \tag{12}$$

where $\|\cdot\|_2 = \|\cdot\|_{L^2(\mathbb{R}^2)}$. Our aim is to estimate $\|f_k - f\|_{L^2(\mathbb{R}^2\times[t_k,t_{k+1}])}$, where f_k is defined in (11) and constant with respect to time.

First of all, we note that K_0 in (9) is a convolution operator whose norm, by Young's inequality, is bounded by 1:

$$\|K_0\|_{L^2\to L^2} \leqslant \|k_0\|_{L^1(\mathbb{R}^2)} = \int_{\mathbb{R}^2} \frac{\exp\left(-\frac{x^2+y^2}{4\Delta t}\right)}{4\pi\,\Delta t}\,\mathrm{d}x\,\mathrm{d}y = 1. \tag{13}$$

The kernel of the convolution operator K_1 in (9) is given by

$$\begin{aligned} k_1(x, y) &= \int_0^{\Delta t} K(x, y, \Delta t - \tau)\,\mathrm{d}\tau \\ &= \int_0^{\Delta t} \frac{\exp\left(-\frac{x^2+y^2}{4(\Delta t-\tau)}\right)}{4\pi(\Delta t - \tau)}\,\mathrm{d}\tau = \frac{1}{4\pi}\int_{\frac{x^2+y^2}{4\Delta t}}^{\infty} \frac{\mathrm{e}^{-s}}{s}\,\mathrm{d}s = \frac{1}{4\pi}\Gamma\left(0, \frac{x^2+y^2}{4\Delta t}\right), \end{aligned}$$

where Γ is the incomplete gamma function ([2]). Hence,

$$\begin{aligned} \|K_1\|_{L^2\to L^2} \leqslant \|k_1\|_{L^1(\mathbb{R}^2)} &= \frac{1}{4\pi}\int_{\mathbb{R}^2} \Gamma\left(0, \frac{x^2+y^2}{4\Delta t}\right)\mathrm{d}x\,\mathrm{d}y \\ &= \frac{1}{2}\int_0^{\infty} \Gamma\left(0, \frac{r^2}{4\Delta t}\right) r\,\mathrm{d}r = \Delta t\int_0^{\infty} \Gamma(0, y)\,\mathrm{d}y = \Delta t, \end{aligned}$$

where the last equality, together with the definition of Γ, can be found in [2, p 262]. We also observe that

$$\nabla k_1(x, y) = -\frac{1}{8\pi}\int_0^{\Delta t} \frac{(x, y)}{(\Delta t - \tau)^2} \exp\left(-\frac{x^2+y^2}{4(\Delta t-\tau)}\right)\mathrm{d}\tau,$$

and

$$\|\nabla k_1\|_{L^1(\mathbb{R}^2)} = \frac{1}{8\pi}\int_{\mathbb{R}^2}\int_0^{\Delta t} \frac{(x^2+y^2)^{1/2}}{(\Delta t-\tau)^2} \exp\left(-\frac{x^2+y^2}{4(\Delta t-\tau)}\right)\mathrm{d}\tau\,\mathrm{d}x\,\mathrm{d}y$$

$$= \frac{1}{8\pi}\int_0^{2\pi}\int_0^{\infty}\int_0^{\Delta t}\frac{r}{s^2}\exp\left(-\frac{r^2}{4s}\right) r\,\mathrm{d}\theta\,\mathrm{d}r\,\mathrm{d}\tau$$
$$= \frac{1}{4}\int_0^{\infty}\int_0^{\Delta t}\frac{r^2}{s^2}\exp\left(-\frac{r^2}{4s}\right)\mathrm{d}s\,\mathrm{d}r = \sqrt{\pi\,\Delta t}.$$

Hence, we have

$$\|K_1\phi\|_{H^1(\mathbb{R}^2)} \leqslant (\Delta t + \sqrt{\pi\,\Delta t})\|\phi\|_2.$$

Due to the compactness of the inclusion of $H^1(\mathbb{R}^2)$ into $L^2(\mathbb{R}^2)$, K_1 is a compact linear operator from $L^2(\mathbb{R}^2)$ into itself. This implies that for every positive α, the Tikhonov functional

$$J_\alpha(\phi) := \|K_1\phi + K_0 g_k - g_{k+1}\|_2^2 + \alpha\|\phi\|_2^2$$

has a unique minimum $f_k \in L^2(\mathbb{R}^2)$ (see, for example [5, section 2.2]). This minimum is the unique solution of the normal equation

$$\alpha f_k + K_1^* K_1 f_k = K_1^*(g_{k+1} - K_0 g_k). \tag{14}$$

The solution f_k of the normal equation (14) can be written as

$$f_k = R_\alpha(g_{k+1} - K_0 g_k),$$

where

$$R_\alpha := (\alpha I + K_1^* K_1)^{-1} K_1^*.$$

By theorem 2.12 in [5], it follows that

$$\|R_\alpha\|_{L^2\to L^2} \leqslant \frac{1}{2\sqrt{\alpha}}. \tag{15}$$

We make the following assumptions on the true solution f:

(H1) The function f is continuously differentiable with respect to t, and there is a function $\psi_1 \in L^2(\mathbb{R}^2)$ such that

$$|f_t(\xi,\eta,\tau)| \leqslant \psi_1(\xi,\eta), \quad \text{for every} \quad (\xi,\eta)\in\mathbb{R}^2, \tau\in[0,T].$$

(H2) For each $t\in[0,T]$, there is a function $\psi_2(x,y,t)\in L^2(\mathbb{R}^2)$ such that

$$f = K_1^*\psi_2.$$

Moreover,

$$\|\psi_2(\cdot,\cdot,t)\|_2 \leqslant \Psi_2 \qquad \text{for every} \quad t\in[0,T].$$

The first part of (H2) assumes that $f(x,y,t)$ is in the range of the operator K_1^*, which makes it somewhat smooth. The smoothness depends on the size of the time step $(t_{k+1}-t_k)$; the bigger the time step, the smoother the f. Therefore, if the sampling rate is high, we expect that this part of (H2) will not play a very strong role. The second part of (H2) controls the norm of $f(x,y,t)$.

We write (9) as

$$0 = u_{k+1} - K_0 u_k - \int_0^{\Delta t}\int K(x-\xi, y-\eta, \Delta t-\tau) f(\xi,\eta,t_k+\tau)\,\mathrm{d}\xi\,\mathrm{d}\eta\,\mathrm{d}\tau.$$

If we add to both sides of this equality the term $K_1 f(x,y,t_{k+1})$, hit both sides by K_1^* and add $\alpha f(x,y,t_{k+1})$, we get

$$(\alpha I + K_1 K_1^*) f(x,y,t_{k+1}) = K_1^*(u_{k+1} - K_0 u_k) + \alpha f(x,y,t_{k+1})$$
$$- K_1^*\left(\int_0^{\Delta t}\int K(x-\xi, y-\eta, \Delta t-\tau)[f(\xi,\eta,t_k+\tau)\right.$$
$$\left. - f(\xi,\eta,t_{k+1})]\,\mathrm{d}\xi\,\mathrm{d}\eta\,\mathrm{d}\tau\right).$$

If we compare this with the normal equation $(\alpha I + K_1 K_1^*) f_k = K_1^*(g_{k+1} - K_0 g_k)$ and use assumption (H2), we get

$$f(x, y, t_{k+1}) - f_k(x, y) = R_\alpha((u_{k+1} - g_{k+1} - K_0(u_k - g_k)) + \alpha\psi_2(x, y, t_{k+1}) - h(x, y)), \tag{16}$$

where

$$h(x, y) = \int_0^{\Delta t} \int K(x - \xi, y - \eta, \Delta t - \tau)[f(\xi, \eta, t_k + \tau) - f(\xi, \eta, t_{k+1})]\, \mathrm{d}\xi\, \mathrm{d}\eta\, \mathrm{d}\tau.$$

By (12) and (13), we have

$$\|u_{k+1} - g_{k+1} - K_0(u_k - g_k)\|_2 \leqslant 2\delta, \tag{17}$$

while, from assumption (H2) we get

$$\|\psi_2(\cdot, \cdot, t_{k+1})\|_2 \leqslant \Psi_2. \tag{18}$$

We need next to estimate $\|h\|_2$. By assumption (H1) we can write

$$\begin{aligned}
|h(x, y)| &\leqslant \int_0^{\Delta t} \int_{\mathbb{R}^2} K(x - \xi, y - \eta, \Delta t - \tau)|f(\xi, \eta, t_k + \tau) - f(\xi, \eta, t_k + \Delta_t)|\, \mathrm{d}\xi\, \mathrm{d}\eta\, \mathrm{d}\tau \\
&= \int_0^{\Delta t} \int_{\mathbb{R}^2} K(x - \xi, y - \eta, \Delta t - \tau)|f_t(\xi, \eta, t_k + \Delta t - \theta\tau)|(\Delta_t - \tau)\, \mathrm{d}\xi\, \mathrm{d}\tau \\
&\leqslant \int_0^{\Delta_t} \int_{\mathbb{R}^2} K(x - \xi, \Delta_t - \tau)\psi_1(\xi, \eta)(\Delta_t - \tau)\, \mathrm{d}\xi\, \mathrm{d}\tau.
\end{aligned}$$

Hence, by Young's inequality,

$$\begin{aligned}
\|h\|_2 &\leqslant \|\psi_1\|_2 \left\| \int_0^{\Delta t} K(\cdot, \Delta t - \tau)(\Delta t - \tau)\, \mathrm{d}\tau \right\|_{L^1(\mathbb{R}^2)} \\
&= \|\psi_1\|_2 \left(\frac{1}{4\pi} \int_{\mathbb{R}^2} \int_0^{\Delta t} \exp\left(-\frac{x^2 + y^2}{4(\Delta_t - \tau)} \right) \mathrm{d}\tau\, \mathrm{d}x\, \mathrm{d}y \right) = \|\psi_1\|_2 \frac{\Delta t^2}{2}.
\end{aligned} \tag{19}$$

Finally, by putting together (16), (15), (17), (18) and (19), we get

$$\|f_k(\cdot) - f(\cdot, t_{k+1})\|_2 \leqslant \frac{1}{2\sqrt{\alpha}} \left(2\delta + \frac{\Delta t^2}{2} \|\psi_1\|_2 + \alpha\Psi_2 \right).$$

This estimate provides a bound for the difference between the estimated source in the interval $[t_k, t_{k+1})$ with the true source at time t_{k+1}. The bound depends on the noise level δ and the time step Δt, in addition to the bounds on the smoothness of the true source.

Now, if we denote

$$\tilde{f}(x, y, t) = f_k(x, y) \quad \text{for} \quad t \in [t_k, t_{k+1}),$$

we have

$$\begin{aligned}
\|\tilde{f} - f\|^2_{L^2(\mathbb{R}^2 \times [0,T])} &= \sum_{k=0}^{N-1} \int_{t_k}^{t_{k+1}} \int_{\mathbb{R}^2} (\tilde{f}(x, y) - f(x, y, t))^2\, \mathrm{d}x\, \mathrm{d}y\, \mathrm{d}t \\
&\leqslant 2 \sum_{k=0}^{N-1} \int_{t_k}^{t_{k+1}} \|\tilde{f}(\cdot) - f(\cdot, t_{k+1})\|_2^2\, \mathrm{d}t \\
&\quad + 2 \sum_{k=0}^{N-1} \int_{t_k}^{t_{k+1}} \int_{\mathbb{R}^2} (f(x, y, t_{k+1}) - f(x, y, t))^2\, \mathrm{d}x\, \mathrm{d}t \\
&\leqslant \frac{T}{2\alpha} \left(2\delta + \frac{\Delta t^2}{2} \|\psi_1\|_2 + \alpha\Psi_2 \right)^2 + 2T \frac{\Delta t^2}{3} \|\psi_1\|_2^2.
\end{aligned}$$

The last estimate suggests that in order for the method to converge, we must choose the regularization parameter α to be of the order of $\sqrt{\delta}$. When so chosen, as the noise level δ and the time step Δt approach 0, the true source is recovered.

6. Numerical experiment

We next investigate the properties of the source reconstruction procedure in numerical calculations. In order to do this, we need to develop a forward solver. Additionally, we shall also study the regularization properties so that we can choose an appropriate parameter.

6.1. Forward problem

We start by discretizing the problem. We consider a finite domain $\Omega = [-1, 1] \times [-1, 1]$ to represent the region to be inspected. It is assumed that the source is compactly supported away from the boundaries of Ω. The region is sampled at increments of $\Delta x = 2/N$; thus the mesh points are

$$x_i = -1 + (i-1)\Delta x, \quad y_j = -1 + (j-1)\Delta x, \quad (i, j) = 1, 2, \ldots, N.$$

The operators K_0 and K_1 are convolutions and will be evaluated using the fast Fourier transform. The operator K_0 has a continuous kernel. To approximate it, we simply sample the values of $k_0(x, y)$ at the points (x_i, y_j). The operation with K_0 is now a discrete convolution, and the integration has been replaced by trapezoidal rule.

The operator K_1 has a kernel with a logarithmic singularity at $(0, 0)$. To see this, consider

$$k_1(x, y) = \int_0^{\Delta t} K(x, y, \Delta t - \tau)\, \mathrm{d}\tau = \int_0^{\Delta t} \frac{\mathrm{e}^{(x^2+y^2)/4(\Delta t-\tau)}}{4\pi(\Delta t - \tau)}\, \mathrm{d}\tau.$$

After a change of variables, we can rewrite $k_1(x, y)$ as

$$k_1(x, y) = \frac{1}{4\pi} \int_{\frac{(x^2+y^2)}{4\Delta t}}^{\infty} \frac{\mathrm{e}^{-s}}{s}\, \mathrm{d}s = \frac{1}{4\pi} E_1\left(\frac{(x^2 + y^2)}{4\Delta t}\right),$$

where $E_1(z)$ is the exponential integral [2]. Using the expansion for $E_1(z)$ given in [2] section 5.1.11, we obtain

$$k_1(x, y) = \frac{1}{4\pi}\left(-\gamma - \log\frac{x^2 + y^2}{4\Delta t} - \sum_{n=1}^{\infty} \frac{(-1)^n \left(\frac{x^2+y^2}{4\Delta t}\right)^n}{nn!}\right),$$

where γ is Euler's constant. The logarithmic singularity is evident in the above expression.

To handle the integration of the kernel, we implement the approach proposed by Aguillar and Chen [1]. Since $k_1(x, y)$ is well defined at all points except $(0, 0)$, all that is needed is to alter the matrix corresponding to the values of $k_1(x, y)$ at sample points (x_i, y_j) at the origin. Following the formula described in [1], we replace $k_1(0, 0)$ by

$$\frac{1}{4\pi}(-\gamma - 2(\log \Delta x + c_1) + \log 4\Delta t),$$

where $c_1 = -1.310\,532\,925\,911\,5095$. The convolution can proceed as before. The error committed at the singularity is $O(\Delta x^4)$, which is negligible compared to that of the trapezoidal rule.

For our numerical experiments, we choose $\Delta t = 0.01$, and $\Delta x = 2/256$. The full surface temperature data will consist of 20 samples of surface temperature u at time interval Δt; each will be a matrix of 256×256.

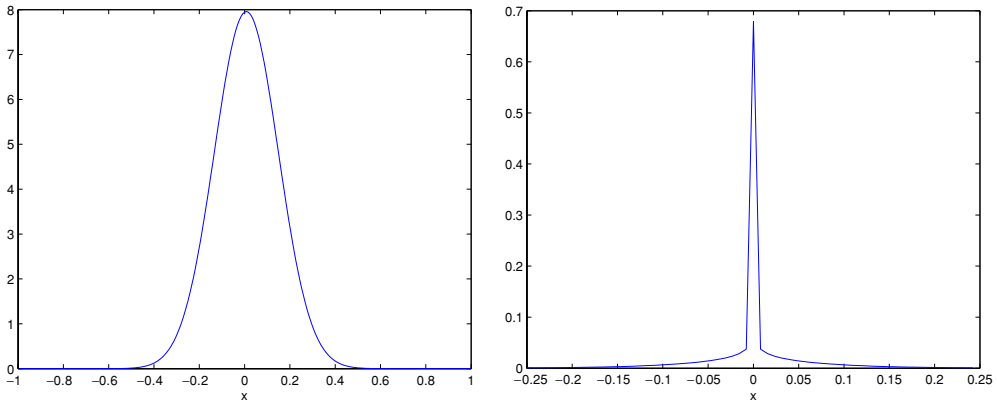

Figure 3. The convolution kernel $k_0(x, 0)$ is shown on the left. On the right is a representation of kernel $k_1(x, 0)$ after the singular integral approximation is implemented. The discrete convolution will be performed against these kernels.

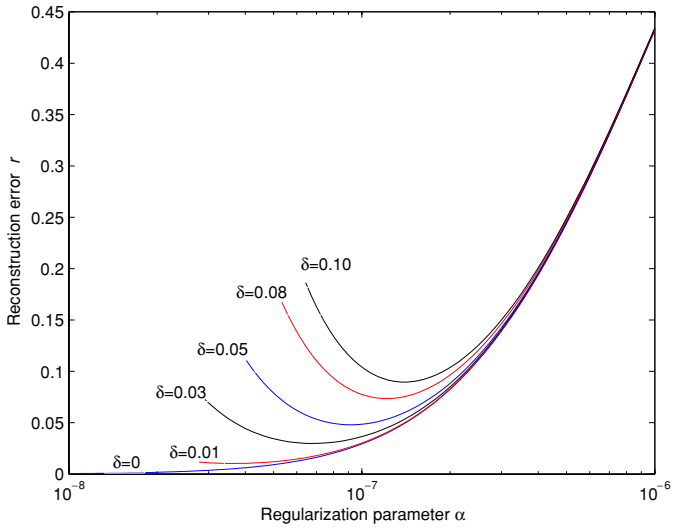

Figure 4. The graphs of reconstruction error as a function of regularization parameter for different noise levels for a given heat source. Shown are the graphs for noise levels $\delta_2 = 0, 0.01, 0.03, 0.05, 0.08, 0.10$. The value of α corresponding to the lowest reconstruction error moves to the right as noise level is increased.

(This figure is in colour only in the electronic version)

It is instructive to examine the graphs of the convolution kernels k_0 and k_1. Figure 3 shows the convolution kernels after discretization. They represent $k_0(x, 0)$ and $k_1(x, 0)$ as the axes indicate, but in truth, they are the discrete convolution kernels. The inverse problem is basically a deconvolution of data that have been smoothed by kernel k_1. It can be seen from the figure that k_1, because of the logarithmic singularity, is not overly smoothing. Therefore, we expect the inverse problem to be somewhat better behaved, and only a small amount of regularization will be required.

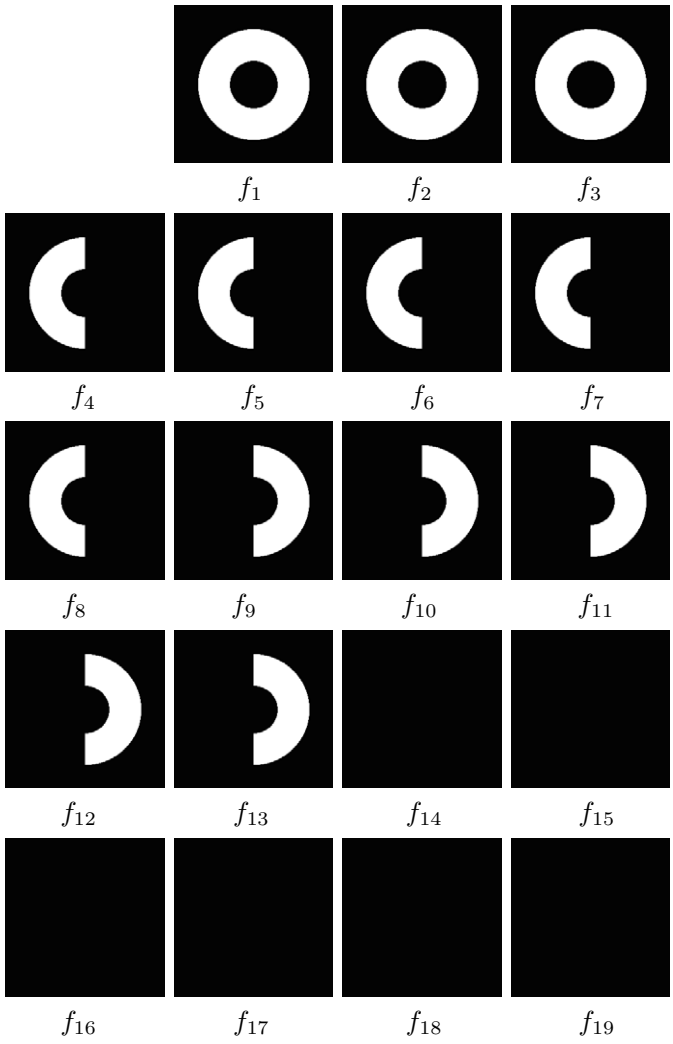

Figure 5. The heat source distributions $f_k(x, y)$ for the time interval $(k-1)\Delta t < t < k\Delta t$. The source distribution is piecewise constant, with light areas corresponding to 1 and dark corresponding to 0. Note that the source is zero for $t > 13\Delta t$.

Having discretized the problem, we can now proceed to generate simulated measured data. We start with source distributions $f_k(x_i, y_j)$, for $k = 1, 2, \ldots, M$. With initial condition $u_0(x_i, y_j) = 0$, we solve for $u_k(x_i, y_j)$ for $k = 1, 2, \ldots, M$ using (10). We will add noise to the data. Our measure of noise is

$$\delta_2 = \frac{\max_k \sum_{i,j} |g_k(x_i, y_j) - u_k(x_i, y_j)|^2}{\max_k \sum_{i,j} |u_k(x_i, y_j)|^2},$$

where $g_k(x_i, y_j)$ is the noise-corrupted version of $u_k(x_i, y_j)$. Noise is generated using a Poisson noise generator, which mimics camera noise.

We remark that we will be using the discretized forward solver in the reconstructions. Thus, the data would have been in the range of the operator had we not added noise. The added noise can be viewed as modelling error plus measurement error. Indeed a more convincing

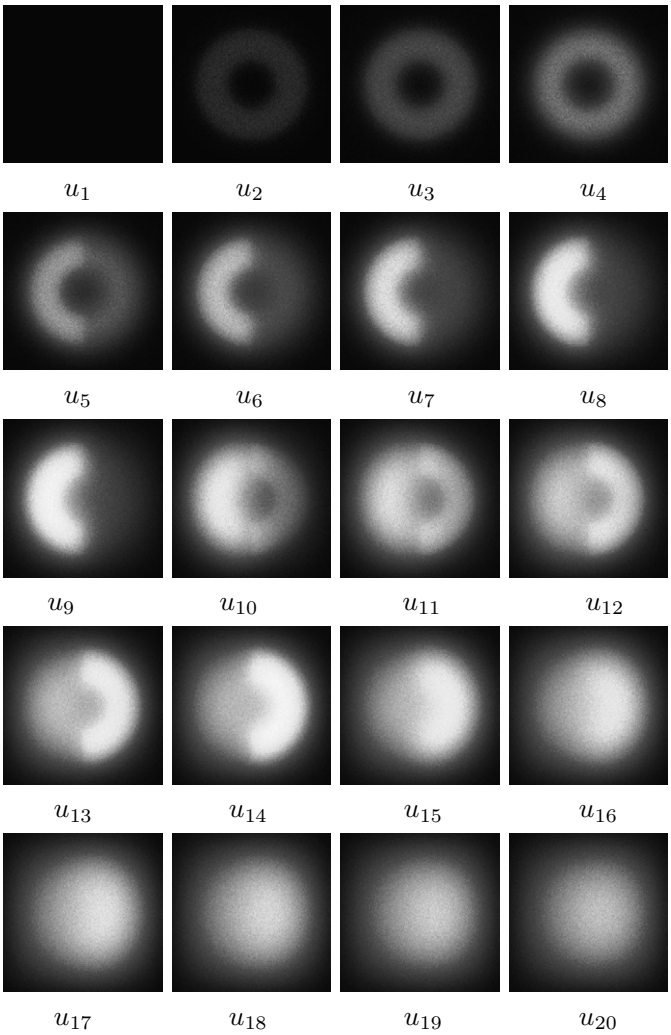

Figure 6. The noisy temperature distribution (data for the inverse problem) at times $t = 0, \Delta t, \ldots, 19\Delta t$. The noise level $\delta_2 = 0.05$. Note that the temperature continues to be nonzero even after the heat source has been turned off.

test is one where data are generated by a full 3D heat conduction simulator, and inversion is done by the reduced 2D method described in this work.

6.2. Regularization

Reconstruction will be done by solving (11) using noisy data $g_k(x_i, y_j)$. As mentioned previously, the inversion is done by a conjugate gradient method. Reconstruction error will be measured by

$$r = \frac{\max_k \sum_{i,j} |\tilde{f}_k(x_i, y_j) - f_k(x_i, y_j)|^2}{\max_k \sum_{i,j} |f_k(x_i, y_j)|^2},$$

where $\tilde{f}_k$ is the reconstruction from noisy data. Note that both δ_2 and r involve squares of errors.

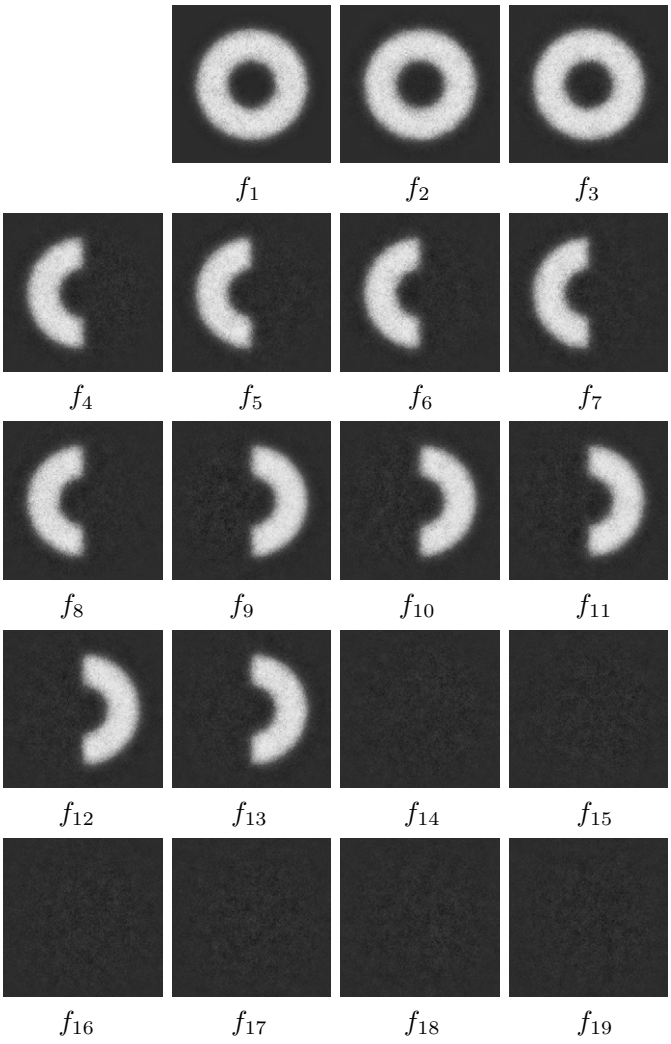

Figure 7. The reconstructed heat source distributions f_k with noise level $\delta_2 = 0.05$. The images should be compared with those in figure 5. Note that the inversion accurately predicts the zero heat source for $t > 13\Delta t$.

As is typical in inverse problems requiring regularization, the optimal value for the regularization parameter is not easy to determine. We do this by optimizing the value for a specific example of a source (shown in figure 5). We make a big leap and assume that the optimal values do not change much from source to source and use the tabulated values as a lookup table for choosing the regularization parameter.

In all our calculations, we take $\Delta t = 0.01$. Recall that under our assumptions, the heat source is assumed to be constant between time samples. In figure 5, we show the heat source distribution as a function of time. The distribution f_k is for $(k-1)\Delta t < t < k\Delta t$. The heat source distribution is used to calculate the temperature distribution via (10). Different levels of noise δ_2 are added to the computed temperature distribution. In figure 6, we show g_k which is the noisy temperature distribution at $t = (k-1)\Delta t$ when $\delta_2 = 0.05$.

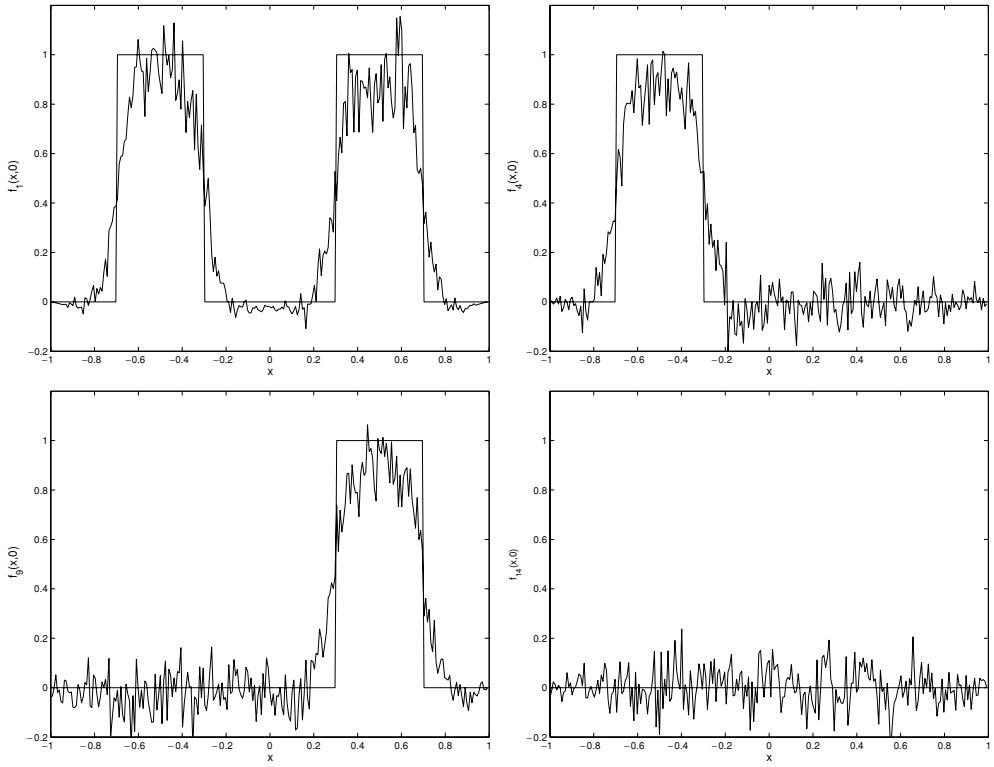

Figure 8. Plots of the recovered heat source at $y = 0$ overlaid on the plots of the true heat source. Shown are $f_k(x, 0)$ for $k = 1, 4, 9, 14$ and their reconstruction from noisy data with $\delta_2 = 0.05$. Except for the rapid oscillation, the recovered heat sources track the true ones well.

Table 1. Numerically derived optimal parameter value as a function of noise level for a specific heat source example.

δ_2	α
0.01	1.6681×10^{-8}
0.03	4.4306×10^{-8}
0.05	6.7342×10^{-8}
0.08	9.3260×10^{-8}
0.10	1.0723×10^{-7}

The next task is to use the simulated data to determine the optimal regularization parameter value. We do this for various levels of noise δ_2 and a range of values for the regularization parameter α. The reconstruction error r is then plotted against α as shown in figure 4. This is done for noise levels $\delta_2 = 0, 0.01, 0.03, 0.05, 0.08, 0.10$. Table 1 lists the optimal parameter value for the noise levels considered.

6.3. Examples

We now show the reconstruction of the heat source from the simulated data in figure 6. The derived optimal regularization parameter is chosen for this noise level. The results are shown in figure 7. The images should be compared with those in figure 5. Note that the reconstructions

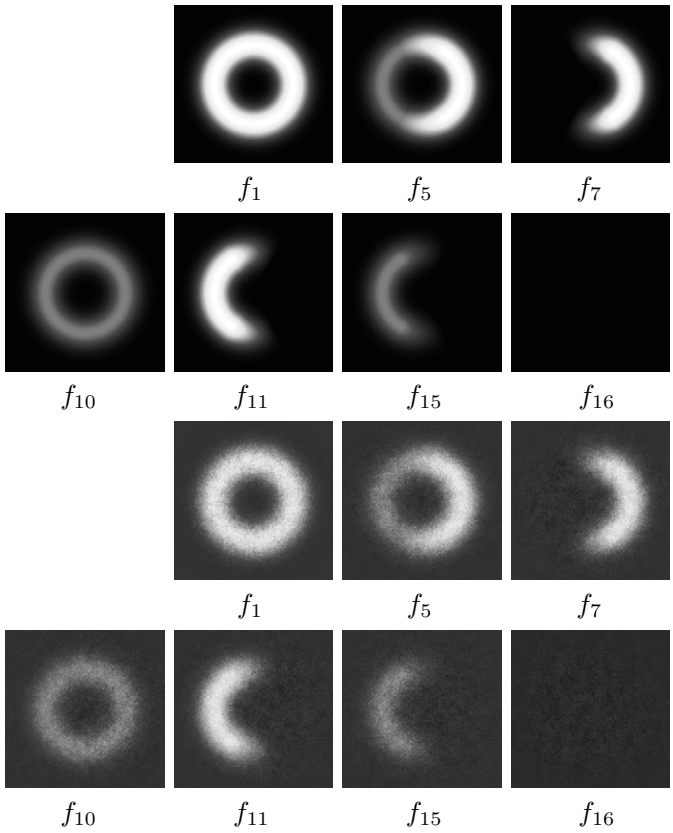

Figure 9. Images of the true heat source and the reconstructed heat source when the source is spatially smooth. The noise level δ_2 is 0.05.

are quite true; the shape of the nonzero components of the heat source is recovered. In particular, the inversion produced heat sources that are near zero for times $t > 13\Delta t$ even though the temperature distribution continues to be nonzero.

To give a better assessment, we take slices of the reconstructed heat source and compare them with those of the true source. Figure 8 shows plots of $f_k(x, 0)$ for $k = 1, 4, 9, 14$. Apart from the oscillations, the recovered heat source tracks the true heat source well.

We also performed an experiment with a smoothed version of the heat source. We display only the true sources and their reconstructions at noise level $\delta_2 = 0.05$. Shown in figure 9 are the images of f_1, f_5, f_7, f_{10}, f_{11}, f_{15}, f_{16} and their reconstructions. Slices of $f_k(x, 0)$ and their reconstructions are shown in figure 10. The regularization parameters used in the reconstruction are those obtained earlier, which are shown to be optimal with respect to the particular heat source in figure 5. The reconstruction error r is tabulated along with the noise level δ_2 in table 2.

We make some observation about the complexity of the algorithm for reconstruction. The most expensive part of the calculation is the matrix inversion needed at each time step. As mentioned earlier, this is done by using a conjugate gradient iteration where each iteration involves a convolution. We observed that convergence is relatively quick, taking between 40 and 60 iterations on a problem involving 256×256 unknowns. Perhaps this process can be

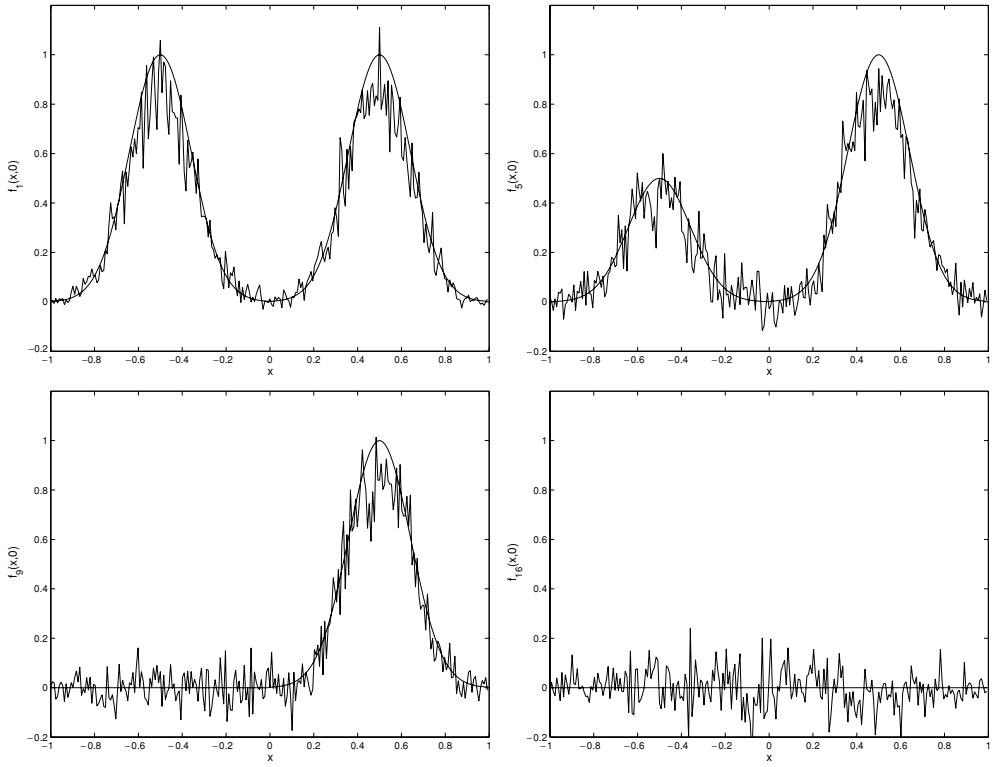

Figure 10. Plots of the recovered heat source at $y = 0$ overlaid on the plots of the true heat source. Shown are $f_k(x, 0)$ for $k = 1, 5, 9, 16$ and their reconstruction from noisy data with $\delta_2 = 0.05$.

Table 2. Reconstruction error versus noise for the case of spatially smooth heat source.

δ_2	r
0.01	0.1084
0.03	0.1334
0.05	0.1455
0.08	0.1647
0.10	0.1774

accelerated by using a preconditioner. A natural candidate for a preconditioner is the inverse operator calculated using a band-limited Fourier inversion of the operator K_1.

7. Discussion

In this work, we considered an inverse problem arising in nondestructive evaluation of spot-welds. The problem reduces to that of determining a time and spatially dependent heat source in a two-dimensional domain from temperature measurements given at fixed time intervals. We devised a simple computational scheme that takes a sequence of temperature readings and estimates the source. The method uses Tikhonov regularization, and is shown to be convergent. Numerical studies with the method show that reconstruction is acceptable even in the presence of noise.

The present study does not address the important issue of how the heat source is related to the quality of a spot-weld. Such a study will involve modelling of heat generation and intimate understanding of the mechanical strength of spot-welds. It is hoped that the results presented in this work will eventually lead to a method for assessing weld quality.

Acknowledgments

Dr Samuel Marin of General Motors first brought the problem described in this work to the attention of FS. We received generous help from him and Dr Cameron Dasch, also of GM, during the course of this work. Some of the work was completed during FS's visit to Istituto per le Applicazioni del Calcolo in Florence, Italy. He thanks the institute for the hospitality during his visit. The research of FS is partially supported by NSF grant no DMS-0504185. TH held a National Science Foundation Graduate Research Fellowship while this work was conducted.

References

[1] Aguillar J-C and Chen Y 2002 High order corrected trapezoidal quadrature rule for functions with logarithmic singularity in 2-d *Comput. Math. Appl.* **44** 1031–9

[2] Abramowitz M and Stegun I (ed) 1972 *Handbook of Mathematical Functions* (Washington, DC: US Department of Commerce)

[3] Favro L, Han X, Ouyang Z, Sun G, Sui H and Thomas R 2000 IR imaging of cracks excited by an ultrasonic pulse *Thermosense XXII (Proc. SPIE vol 4020)* ed R Dinwiddie and D LeMieux (Bellingham WA: SPIE) pp 182–5

[4] Han X, Favro L, Ouyang Z and Thomas R 2001 Recent developments in thermosonic crack detection *Rev. Prog. QNDE* **21** 552–7

[5] Kirsch A 1996 *An Introduction to the Mathematical Theory of Inverse Problems* (Berlin: Springer)

[6] Ouyang Z, Favro L, Thomas R and Han X 2001 Theoretical modeling of thermosonic imaging of cracks *Rev. Prog. QNDE* **21** 577–81

[7] Zachmanoglou E and Thoe D 1976 *Introduction to Partial Differential Equations with Applications* (Baltimore, MD: Williams & Wilkins)